

Photo-Robotic Positioning for Integrated Optics

Houari Bettahar, Alexis Caspar, Cédric Clévy, Nadège Courjal, and Philippe Lutz

Abstract—High positioning accuracy is a crucial need to perform successfully complex tasks such as micromanipulation and microassembly. This especially enables to provide high performances or to propose new functionalities/products, notably for integrated optical devices. The objective of the letter is to align two optical structures in multi-DOF way with very high accuracy. The originality of the approach relies on robotic positioning associated with the use of interfered reflected light irradiance as a feedback signal rather than transmitted power. Fabry-Perot interference principle is especially used to provide a fast and high accurate measurement. An opto-mechanical model that relates the optical component poses with the interfered reflected light is proposed. Experimental results are investigated based on a robotic multi-DOF platform, used to relatively align an optical component to an optical fiber. The obtained results establish that the model fits with experiments with a standard deviation below 0.0281° . This model associated with an automated positioning strategy shows that it is possible to maximize reflectivity within less than 6 s, including multi-DOF angular misalignments identification and compensation.

Index Terms—Automation at micro-nano scales, micro/nano robots, assembly.

I. INTRODUCTION

INTEGRATED optical systems have emerged over the past decades with an increasing market demand in several application areas such as medical engineering, information technology, production technology. Hybrid integrated optical nano and micro-circuits resulting from the assembly of multiple optical elements have particularly attracted attention, due to their very high interest to concentrate functionalities in very small areas ($<1 \text{ mm}^2$) [1], [2]. Hybrid integrated optical nano and micro-circuits usually result from successive clean room processes, so that their optical characteristics are tested only at the end of the process flow. This leads to high yield losses. A promising alternative is to manufacture each of the optical building components separately and optimize their optical performances through robotic micro-assembly. This approach appears as promising because it provides high performances or

Manuscript received March 01, 2016; accepted June 23, 2016. Date of publication July 09, 2016; date of current version August 05, 2016. This paper was recommended for publication by Associate Editor M. Rakotondrabe and Editor Y. Sun upon evaluation of the reviewers comments. This work was supported in part by the Franche-Comté region, nano-robotic project (2015C-5709) supported by the Labex ACTION project (contract ANR-11-LABX-0001-01) and in part by the French RENATECH network through its FEMTO-ST technological facility.

H. Bettahar, C. Clévy, and P. Lutz are with the FEMTO-ST Institute, AS2M Department, University Bourgogne Franche-Comté, University de Franche-Comté/CNRS/ENSMM, 25000 Besançon, France (e-mail: houari.bettahar@femto-st.fr; cclevy@femto-st.fr; philippe.lutz@femto-st.fr).

A. Caspar and N. Courjal are with the FEMTO-ST Institute, Optics Department, University Bourgogne Franche-Comté, University de Franche-Comté/CNRS/ENSMM, 25000 Besançon, France (e-mail: alexis.caspar@femto-st.fr; nadège.courjal@femto-st.fr).

Color versions of one or more of the figures in this letter are available online at <http://ieeexplore.ieee.org>.

Digital Object Identifier 10.1109/LRA.2016.2589319

propose new optical functionalities and products [3], [4]. This approach relies on the ability of accurate multi-degree(s) of freedom (DOF) positioning of optical components. Sub- μ accuracy is typically targeted [5].

There are two main alignment approaches: passive alignment and active alignment [6], [7], [8], [9]. Hybrid forms exist as well, where passive alignment is performed in some DOF and active alignment in the other(s) [10] or where the pre-alignment is used passively, followed by active fine alignment [11].

In passive alignment, no feedback based on the optical coupling is used, the photonic components are passive during alignment. The accuracy of passive alignment techniques closely depends on the alignment device. Despite it is potentially quicker and costless, it generally reaches a lateral accuracy of about $1 \mu\text{m}$ [12], [13].

In contrast, in active alignment technique, the optical system properties are used as a feedback for closed loop control. Motion stages are employed to adjust the positions of the optical component in order to obtain the high alignment accuracy [8]. As a result of the closed-loop control, the lateral alignment accuracy is much more satisfactory, and can typically reach 100 nm. The feedback signal is usually the transmission power measured by an optical power meter [14]. It is one-dimensional (1-D) alignment process, for misalignments on multiple dimensions, it has to deal with one dimension after another. This approach is generally time-consuming and especially difficult for dealing with angular misalignments. An other alternative consists in using a proprioceptive sensory feedback such as cameras [15]. The components geometrical informations are used for closed loop control to achieve accurate multi-DOF positioning. However, a good geometrical alignment does not guarantee an optimized optical function and a high multi-DOF positioning accuracy.

The objective of the paper is to accomplish high accurate active multi-DOF angular alignment and positioning of optical structures, especially for nanophotonic components. It relies on interfered reflected light irradiance for closed loop control rather than the transmitted power signal. Active alignment of optical components generally generates Fabry-Perot cavity, due to air gap between the interfaces. In this paper we propose to use this Fabry-Perot interference principle for fast and accurate angular measurement. The key is to derive an opto-mechanical model which relates an optical component poses with the interfered reflected irradiance. Based on this knowledge (measurement, model), these misalignments can then be compensated rapidly to maximize the reflected irradiance, and to provide an automated high accuracy multi-DOF positioning. The paper is organized as follows. Section II describes the micro-photonic component and its process of fabrication. Section III models angular positioning and the interfered reflected light irradiance relationship based on Fabry-Perot interference. Section IV presents the dedicated experimental multi-DOF platform. Section V investigates

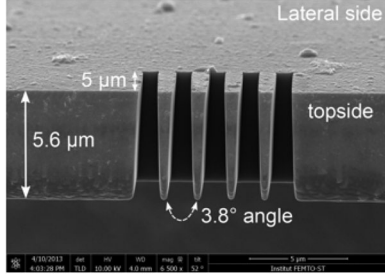


Fig. 1. A SEM view of a Bragg mirror integrated in a LiNbO₃ waveguides. The angles between the walls of the Bragg mirror cause a significant reduction of reflectivity [16].

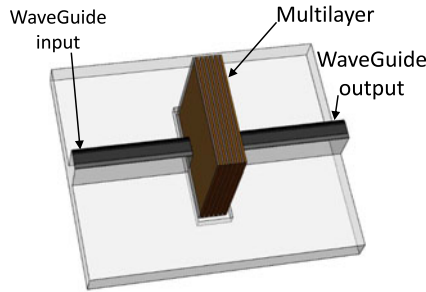


Fig. 2. Post-integration of a multilayer in an optical waveguide.

and quantifies experimentally model performances and automated high positioning accuracy. Section VI concludes the paper.

II. THE PHOTONIC COMPONENT

In integrated optics, many features are obtained through cleanroom process and are tested only at the end of the workflow, which can generate defects altering the optical performance. As an example, it can be seen in Fig. 1 that a short Bragg mirror inscribed in an optical waveguide ineluctably shows angles due to the fabrication process, inducing losses and low reflectivity [16]. A highly reflective multilayer inserted inside the waveguide can advantageously replace the inscribed Bragg mirror and consequently enhance the reflectivity, as depicted in Fig. 2. Such an approach requires an accurate active photonic positioning to reduce the optical losses due to parasitical angles. Similarly, micrometer-thin planar optical waveplates controlling the polarization of light appear as an attractive alternative to millimeter-long integrated waveplates [17]. In both of these two examples, there is a need in accurately aligning thin-plates with optical waveguides.

Here we propose an easy-to-implement protocol to dynamically control the alignment of thin plates with waveguides so as to provide high optical performances. For the sake of illustration, we have produced a $4.95\ \mu\text{m}$ thin plate through the lapping and polishing of birefringent X-cut LiNbO₃ wafers. These thin plates were then diced into $300\ \mu\text{m}$ wide squares by means of a circular precision saw, as described in reference [16] and as schematically depicted in Fig. 3(a). A corresponding SEM view of one optical component (thin plate) is depicted in Fig. 3(b).

In what follows we describe the protocol of angular photonic positioning of the optical component relative to the optical fiber.

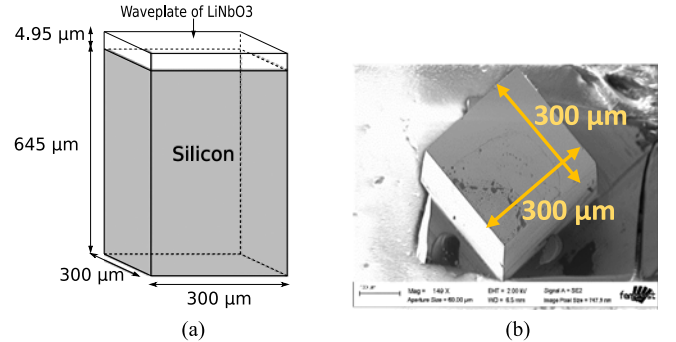


Fig. 3. (a) Photonic component model, (b) A SEM image of one photonic component dedicated for the experimental investigation.

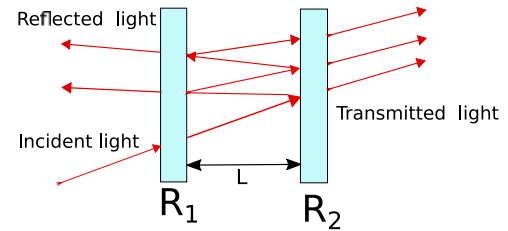


Fig. 4. Schematic diagram representing the interferences in a Fabry-Perot optical cavity due to a thin film of air bounded between R_1 and R_2 .

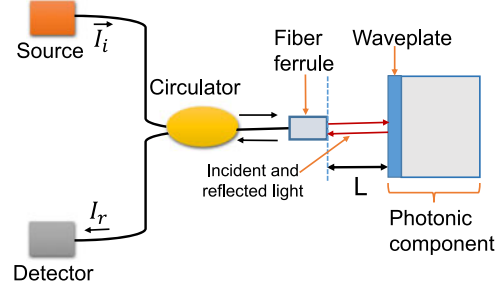


Fig. 5. Experimental setup for measuring the reflected light from the system behaving as a Fabry-Perot interferometer.

III. THE OPTO-MECHANICAL MODEL

The phenomenon of interference of light is used in many high precision measuring systems and sensors. The Fabry-Perot interference compared with other interferences, produces constructive interference with very high measurement resolution. For this sake, the Fabry-Perot interference principle is chosen for angular misalignment identification. More precisely, we propose to exploit the Fabry-Perot optical cavity between the end of fiber and optical component. The system behaves like the Fabry-Perot interferometer as depicted in Fig. 4, where interferences result from the recombination of multiple reflections between the semi-reflective surfaces R_1 (output of the fiber) and R_2 (input of the optical component) respectively. We propose to use an optical circulator as shown in Fig. 5 to measure the interfered reflected response.

Based on the Fabry-Perot interference principle, when the cavity distance is constant and when the wavelength is fixed, the reflected light irradiance is theoretically constant.

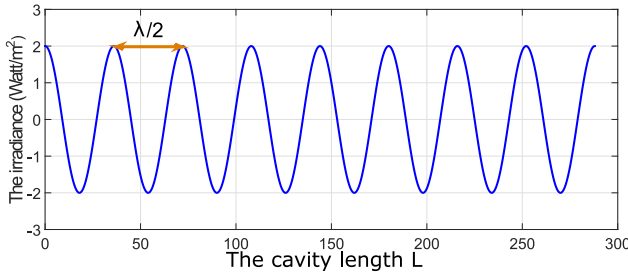


Fig. 6. Reflected irradiance versus Fabry-Perot cavity length L .

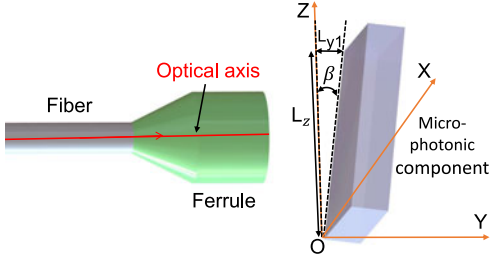


Fig. 7. The β fault angle identification based fiber ferrule light reflection irradiance and micro-photonic component scan. β is the angle between the surface of the optical component and the Z-axis in the (YOZ) plan.

When one of the two plates is moving continuously toward the second one for a certain distance, it generates a continuous cavity distance variation, and this yields an oscillating reflected light irradiance [18]. From the oscillating reflected light irradiance, the cavity distance variation can be calculated. The maxima are obtained each time the cavity length L is multiple of $\lambda/2$. $L_{max,p}$ is the cavity length corresponding to the p th maximum of reflected light irradiance, where p is a natural number, and λ is the light beam wavelength, as shown in Fig. 6 and equation (1):

$$L_{max,p} = \frac{\lambda}{2} \cdot p. \quad (1)$$

This principle is used in this paper to accurately identify angular misalignments. Indeed, if the micro-photonic component has initially a β fault angle (see Fig. 7), then a vertical scan of the micro-photonic component along the Z-axis with a known scan displacement L_z is expected to induce a continuous cavity distance variation L_{y1} . Consequently, it generates an oscillating reflected light irradiance at the same time. From the number of maxima of this oscillating signal, the propagated distance L_{y1} can be evaluated using equation (1) and as shown in Fig. 6. From the assessment of the distance L_{y1} , and for a given vertical scan distance L_z , the angle β (the angle between the surface of the waveplate and the YOZ plan) can be calculated using the following equation:

$$\beta = \arctan \left(\frac{L_{y1}}{L_z} \right). \quad (2)$$

The same steps are followed as previously mentioned for the fault tilt angle θ identification, where θ is the angle between the surface of the optical component and the X-axis in the (XOY) plan.

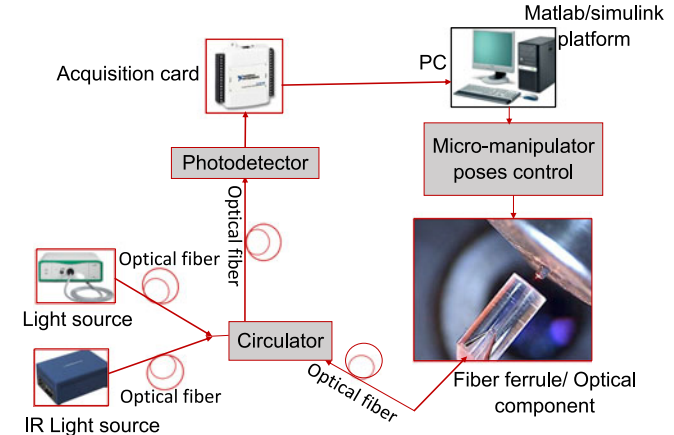


Fig. 8. The photo-robotic scheme for fault angle identification and correction.

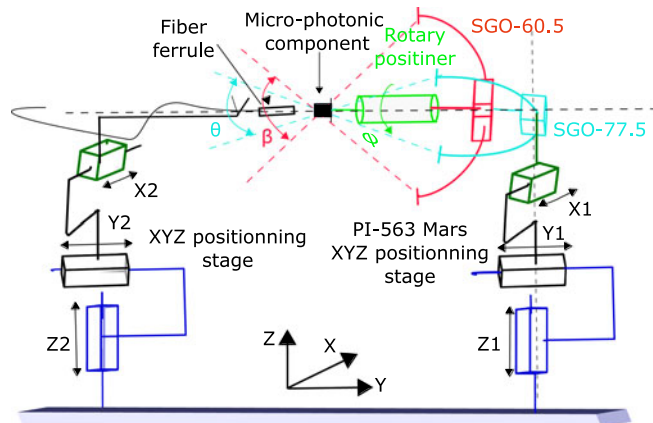


Fig. 9. The kinematic scheme of the proposed robotic micro-manipulator for micro-alignment of micro-optical components.

IV. EXPERIMENTAL PLATFORM

In order to control the position of the photonic component relative to the fiber ferrule, the experimental set up is proposed as schematically depicted in Fig. 8. A 6 DOF nano-manipulator has been designed, to hold the micro-photonic component and control its poses. It comprises P-563 PIMars Nano-positioning stage for the translational motion on X, Y, Z directions, with a maximum displacement range of $300 \mu\text{m}$ each. For rotational motion around Z-axis and X-axis, we use the SGO-60.5 and SGO-77.5 goniometers respectively, which have each a rotating range from -5° to 5° . We use also a rotary positiner for rotation around Y-axis with 360° as a rotating range. Figs. 9 and 10, shows the kinematic model and the experimental workstation of the proposed robotic system.

The optical set up consists of an infrared laser light source (wavelength $\lambda = 1560 \text{ nm}$) connected to a circulator and then to a fiber ferrule. The fiber ferrule is fixed by a holder at the end of the XYZ-positioning stage. The XYZ-positioning stage is fixed in front of the six DOF micro-manipulator. This configuration allows to align and assemble the optical component to the optical fiber ferrule. The reflected irradiance from micro-photonic component through the fiber ferrule is the feedback information for the robotic micro-manipulator poses control.

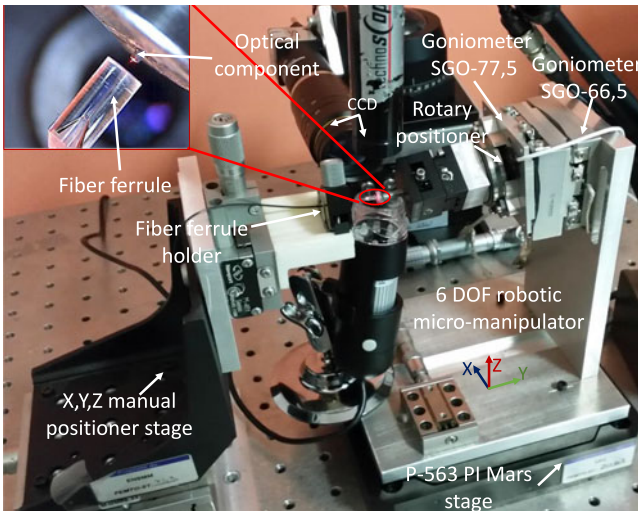


Fig. 10. The experimental set up workstation.

This set up allows light reflection from the photonic component surface through the fiber ferrule, then to the circulator to be acquired by a NATIONAL INSTRUMENT acquisition card, and to be used to control the micro-manipulator poses and then relative position between fiber ferrule/optical component in active way.

V. EXPERIMENTAL RESULTS

A. The Proposed Approach Validation

In this section, the angular misalignment identification based reflected light irradiance presented in Section III is implemented. The experimental set-up and the opto-robotic scheme presented in Section IV are realized using Matlab/Simulink platform. A sampling frequency 100 Hz is used.

The experimental investigations were performed within constant environmental conditions ($T = 20^\circ\text{C}$).

In order to implement the proposed approach, a preliminary experimental investigation is done, it aims to evaluate repeatability of the optical response. By scanning the photonic component along the fiber ferrule core in the same direction of X-axis and Z-axis, the obtained interfered reflected irradiance for two repeated scans along X-direction and also along Z-direction is shown in Figs. 11 and 12 respectively.

The relationship between the oscillation number P , the distance L_{y2} and the angular misalignment θ , is derived by making the micro-photonic component in different unknown angular misalignment poses, then these angles are identified as shown in Fig. 13, for the case of θ misalignment.

The number of oscillations is directly proportional to angular misalignment, the higher the oscillations number, the higher identified angular misalignment.

In order to study the identified angles repeatability, an automated cycle of angular misalignment identification and compensation is used for a repeated experiment of correction and returning back to the initial fault angle for 40 times. The obtained results are illustrated for the identified β and θ angles in

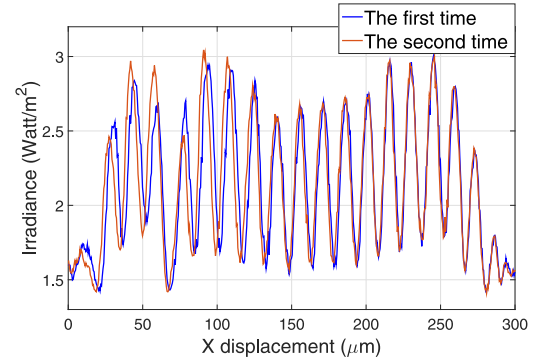


Fig. 11. The reflected light irradiance repeatability investigation for θ misalignment.

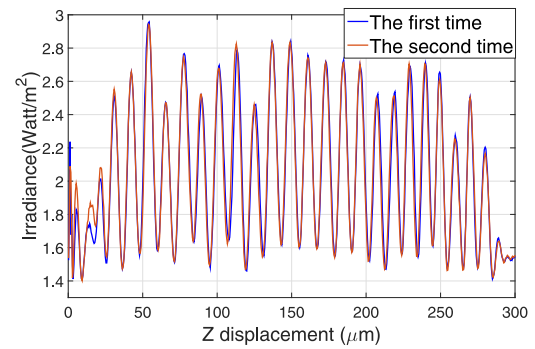


Fig. 12. The reflected light irradiance repeatability investigation for β misalignment.

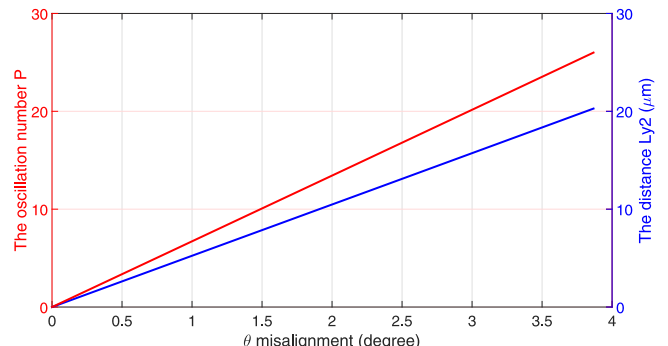


Fig. 13. θ angular misalignment, oscillation number and the distance L_{y2} proportional relationship.

histogram form respectively in Fig. 14. Each histogram represents the number of measures for each identified angle. This representation can significantly show the repeatability distribution of the identified angle, at the same time, the uncertainty is represented in Gaussian distribution form based on the standard deviation and the average value. Table I shows the obtained results for average values, standard deviation and maximum error.

B. Automated High Accuracy Alignment

Once the proposed approach has been validated in term of repeatability and fitness, now it is possible to automate the alignment process. It comprises identification of angular

TABLE I
THE OBTAINED IDENTIFIED RESULTS FOR AVERAGE VALUES, STANDARD DEVIATION AND MAXIMUM ERROR

Identified angle	Average value (degree)	Standard deviation (degree)	Maximum error (degree)
β (degree)	3.5285	0.0281	0.0536
θ (degree)	2.5541	0.0267	0.0614

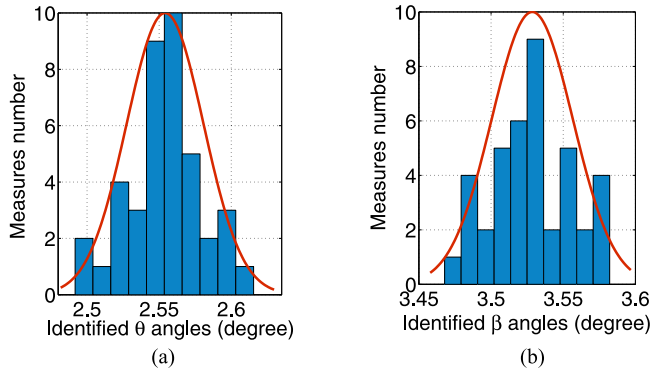


Fig. 14. The repeatability histogram and the incertitude Gaussian distribution for θ and β identified angles.

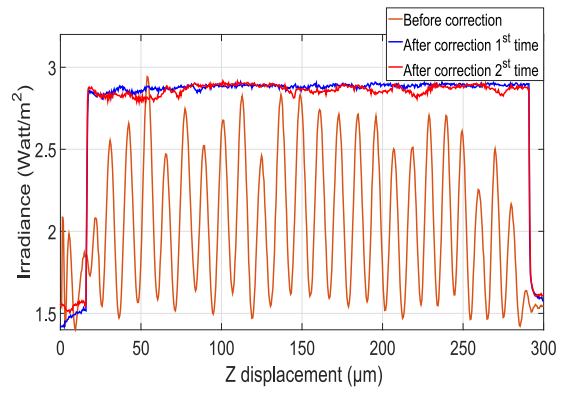


Fig. 16. The reflected light irradiance before and after correction for β misalignment.

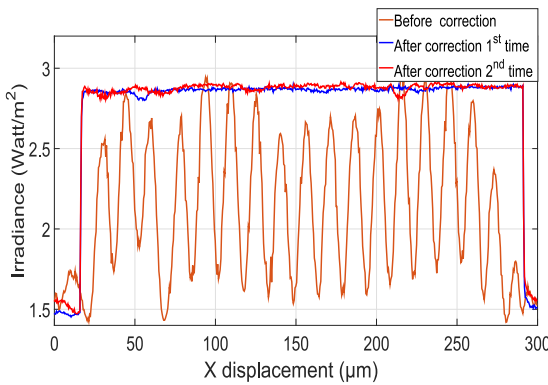


Fig. 15. The reflected light irradiance before and after correction for θ misalignment.

misalignment θ and β and compensation. The obtained identified values for a given angular positions, are $\theta = (2.5541 \pm 0.0267)^\circ$ and $\beta = (3.5285 \pm 0.0281)^\circ$ in elapsed time of 6 s. A second scan along the same direction of X-axis and Z-axis is done to compare the two results before and after correction and another scan along the same direction of X-axis and Z-axis after correction also is done to show the repeatability of the irradiance after correction as shown in Figs. 15 and 16 respectively.

After correction, the fiber and the photonic component are aligned. A scan test along X-direction or Z-direction (depends on which angle we want to correct and align), yields a constant corresponding reflected light irradiance. It means, no Fabry-Perot cavity variation. The irradiance after correction is enough repeatable which means that the external perturbation influences on the irradiance are negligible under constant environmental condition. Any x and z displacements after correction do not affect the reflected irradiance as long as the fiber core is fully face to face with optical component.

The proposed approach offers an automated high alignments accuracy, to maximize the reflected irradiance within less than 6 s.

VI. CONCLUSION

This paper focuses on integrated optics system realised through highly accurate multi-DOF robotic active positioning approach. For this purpose, a two fundamental building components were chosen, a fiber ferrule and a micro-photonic component.

Fabry-Perot cavity interference generally generated between the fiber ferrule and the photonic component, it provides a fast and high accurate measurement was used for accurate and precise angular misalignment identification.

An opto-mechanical model which relates the optical component poses with the interfered reflected light was proposed. It allows to create an optimised optical positioning function and accurate angular misalignment identification and compensation in fast time (less than 6 s). This model was used to achieve automated angular misalignment measurements and compensation.

The angular misalignment identification based interfered reflected light analysis was quantified based on standard deviation for β and θ angles with $\rho_\beta = \pm 0.0281^\circ$ and $\rho_\theta = \pm 0.0267^\circ$ respectively.

A 6-DOF robotic micro-manipulator to hold the photonic component and control its poses was proposed, to achieve complex tasks with high precision, where the reflected light was a closed loop control information.

REFERENCES

- [1] O. Benson, "Assembly of hybrid photonic architectures from nanophotonic constituents," *Nature*, vol. 480, no. 7376, pp. 193–199, 2011.

- [2] P. Rabiei, J. Ma, S. Khan, J. Chiles, and S. Fathpour, "Heterogeneous lithium niobate photonics on silicon substrates," *Opt. Express*, vol. 21, no. 21, pp. 25573–25581, 2013.
- [3] L. Zimmermann, G. B. Preve, T. Tekin, T. Rosin, and K. Landles, "Packaging and assembly for integrated photonics—A review of the epixpack photonics packaging platform," *IEEE J. Sel. Topics Quantum Electron.*, vol. 17, no. 3, pp. 645–651, May/Jun. 2011.
- [4] J. Agnus *et al.*, "Robotic microassembly and micromanipulation at femto-st," *J. Micro-Bio Robot.*, vol. 8, no. 2, pp. 91–106, 2013.
- [5] G. Böttger, D. Weber, F. Scholz, H. Schröder, M. Schneider-Ramelow, and K.-D. Lang, "Fully automated hybrid diode laser assembly using high precision active alignment," in *Proc. SPIE*, vol. 9730, 2016, Art. no. 97300E.
- [6] P. Karioja, J. Ollila, V.-P. Putila, K. Keranen, J. Hakkila, and H. Kopola, "Comparison of active and passive fiber alignment techniques for multi-mode laser pigtailing," in *Proc. 50th Electron. Compon. Technol. Conf.*, 2000, pp. 244–249.
- [7] R. Hauffe, U. Siebel, K. Petermann, R. Moosburger, J.-R. Kropp, and P. Arndt, "Methods for passive fiber chip coupling of integrated optical devices," in *Proc. 50th Electron. Compon. Technol. Conf.*, 2000, pp. 238–243.
- [8] C.-Y. Tseng and J.-P. Wang, "Automation of multi-degree-of-freedom fiber-optic alignment using a modified simplex method," *Int. J. Mach. Tools Manuf.*, vol. 45, no. 10, pp. 1109–1119, 2005.
- [9] R. Zhang and F. G. Shi, "A novel algorithm for fiber-optic alignment automation," *IEEE Trans. Adv. Packag.*, vol. 27, no. 1, pp. 173–178, Feb. 2004.
- [10] M. Kapulainen *et al.*, "Hybrid integration of InP lasers with soi waveguides using thermocompression bonding," in *Proc. 5th IEEE Int. Conf. Group IV Photon.*, 2008, pp. 61–63.
- [11] M. Datta, Z. Hu, and M. Dagenais, "A novel method for fabrication of a hybrid optoelectronic packaging platform utilizing passive-active alignment," *IEEE Photon. Technol. Lett.*, vol. 15, no. 2, pp. 299–301, Feb. 2003.
- [12] B. Li, H. Wirz, and A. Sharon, "Optimizing fiber coupling with a quasi-passive microoptical bench," *J. Microelectromech. Syst.*, vol. 14, no. 6, pp. 1339–1346, 2005.
- [13] J. F. C. van Gurp, M. Tichem, U. Staufer, and J. Zhao, "Passive photonic alignment with submicrometer repeatability and accuracy," *IEEE Trans. Compon., Packag. Manuf. Technol.*, vol. 3, no. 11, pp. 1971–1979, Nov. 2013.
- [14] Y. Zheng and J.-A. Duan, "Alignment algorithms for planar optical waveguides," *Opt. Eng.*, vol. 51, no. 10, 2012, Art. no. 103 401–1.
- [15] A. Kudryavtsev, G. J. Laurent, C. Clévy, B. Tamadazte, and P. Lutz, "Analysis of cad model-based visual tracking for microassembly using a new block set for matlab/simulink," *Int. J. Optomechatronics*, vol. 9, no. 4, pp. 295–309, 2015.
- [16] C. Guyot *et al.*, "Optical characterization of ultra-short bragg grating on ssi lithium niobate ridge waveguide," *Opt. Lett.*, vol. 39, no. 2, pp. 371–374, 2014.
- [17] G. Corrielli *et al.*, "Rotated waveplates in integrated waveguide optics," *Nature Commun.*, vol. 5, 2014, Art. no. 4249.
- [18] S. Pedrotti, *Basic Physical Optics*. Waco, TX, USA: CORD, 2008.